Direct Mapping of Phonon Dispersion Relations in Copper by Momentum-Resolved X-Ray Calorimetry

Ruqing Xu,[1,2] Hawoong Hong,[3] Paul Zschack,[3] and T.-C. Chiang[1,2,*]

[1]*Department of Physics, University of Illinois at Urbana-Champaign, 1110 West Green Street, Urbana, Illinois 61801, USA*
[2]*Frederick Seitz Materials Research Laboratory, University of Illinois at Urbana-Champaign, 104 South Goodwin Avenue, Urbana, Illinois 61801, USA*
[3]*Advanced Phonon Source, Argonne National Laboratory, 9700 South Cass Avenue, Argonne, Illinois 60439, USA*

(Received 23 May 2008; published 19 August 2008)

We have developed a new method of mapping phonon dispersion relations based on momentum-resolved x-ray calorimetry. X-ray scattering intensities are measured at selected points in reciprocal space with suitably chosen polarization configurations; the thermal part of the scattering intensity is extracted by scanning the temperature of the sample. The intensity variations, governed by the phonon populations, are analyzed to yield the energies of the phonons. This method is applied to copper. With high-order effects under control, the results are in excellent agreement with the known phonon dispersion relations.

DOI: 10.1103/PhysRevLett.101.085504 PACS numbers: 63.20.dd, 61.05.C−

Phonon dispersion relations in crystalline materials are a manifestation of the interatomic bonding forces; as such, they play a fundamental role in many physical effects and phenomena. Efficient determination of these relations is important for the advancement of materials physics. We report herein a new *direct* method of mapping phonon dispersion relations and demonstrate the methodology with a study of copper (Cu) as a model system. Presently, there are two major techniques available for *direct* mapping of phonon dispersion relations: inelastic neutron scattering (INS) [1] and inelastic x-ray scattering (IXS) [2–4]. There also exists an *indirect* method based on x-ray thermal diffuse scattering (TDS) [5–7]. Each of these techniques has its advantages and drawbacks, depending on the systems and problems of interest. For instance, INS generally requires large single crystals and is not applicable to materials with a high neutron absorption cross section. IXS is free from these limitations, but it has a very low data acquisition rate—usually hours for a single data point. The method of TDS typically involves two-dimensional imaging of the scattering intensities along a number of different directions; fitting of the intensity patterns using a force constant model yields the phonon dispersion relations. Because of the fitting involved, the answers can depend on the model chosen; thus, this indirect method is susceptible to systematic errors. However, the data acquisition rate is very high—seconds or minutes for a complete analysis. The TDS method is also amenable to small crystals.

The new method is essentially a calorimetric measurement carried out in reciprocal space based on x-ray TDS measurements. Selected points in k space are singled out by the scattering geometry as in IXS. The temperature dependence of the x-ray scattering intensity at each point is recorded. Since this intensity variation is determined by the phonon populations, a straightforward analysis yields the phonon energies of interest. Energy analysis as in IXS is not required, and thus the detection efficiency is high. At the same time, no force constant modeling is required either.

Our experiment was performed at sector 33-ID, Advanced Photon Source, Argonne National Laboratory. A Cu single crystal with a (110) surface was prepared by mechanical polishing to a mirror finish, followed by electrochemical etching to remove a mechanically damaged surface layer. It was mounted on a sample holder made of copper by mechanical anchoring, and a layer of high-conductivity thermal grease was applied to enhance the thermal contact. The sample holder was coupled via an indium foil to the cold end of a closed-cycle He refrigerator. A heating coil on the refrigerator end, connected to a power supply and a feedback system, provided temperature control. The temperature of the sample was determined by a silicon diode buried directly underneath the sample. The entire assembly was enclosed in a vacuum shroud equipped with beryllium windows. A turbo pump ran continuously to maintain a vacuum around the sample. The refrigerator containing the sample assembly was mounted on a four-circle kappa diffractometer. The incident x-ray beam, with a cross section of 0.5 mm $\times$ 0.5 mm and an energy of 8.0 keV, was monitored by a He gas ion chamber. The scattered beam was defined by a pair of slits and detected by a scintillation detector.

The Cu crystal was oriented and indexed by its Bragg peaks. During the x-ray measurement, the sample temperature was slowly varied between 10 and 200 K to allow near thermal equilibrium at all times, while the diffractometer was moved to various points for scattered intensity measurements. Thermal expansion of the Cu crystal lattice led to slight movements of the Bragg peaks. This was taken into account in setting the diffractometer for selected momentum transfers relative to the crystal. Likewise, thermal

 © 2008 The American Physical Society

expansion of the refrigerator was measured and compensated for by mechanical adjustments.

Figure 1(a) shows the measured x-ray intensity as a function of sample temperature at momentum transfer $\mathbf{q} = (1.1, 1.1, 1.1)$, measured in units of $2\pi/a$, where a is the lattice constant of Cu. The intensity shows substantial temperature dependence, as expected. Theoretically, the TDS intensity is given by

$$I(\mathbf{q}) \propto f^2 e^{-2M} \sum_{j=1}^{3} \frac{1}{\omega_{\mathbf{q},j}} \coth\left(\frac{\hbar\omega_{\mathbf{q},j}}{2k_B T}\right)(\mathbf{q}\cdot\mathbf{e}_{\mathbf{q},j})^2 + \cdots, \tag{1}$$

where the leading term comes from first-order scattering, and the rest (not shown) comes from high-order scattering [6–9]. In Eq. (1), f is the (temperature-independent) atomic form factor, $2M$ is the Debye-Waller factor, and

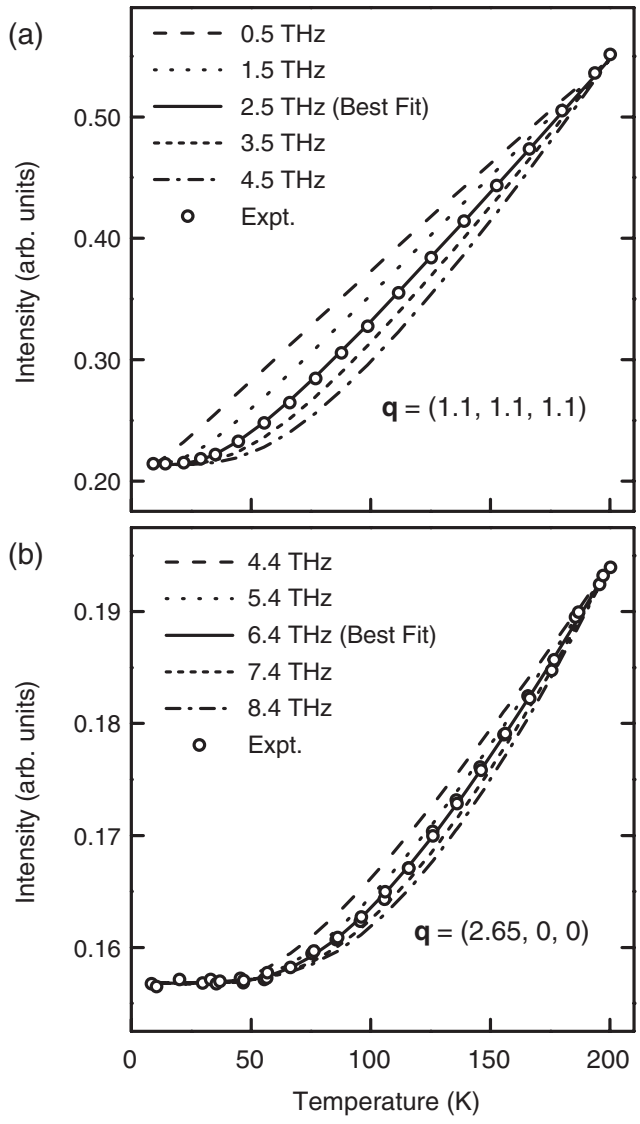

FIG. 1. Experimental and calculated TDS intensities as a function of temperature for $\mathbf{q}$ at (a) (1.1, 1.1, 1.1) and (b) (2.65, 0, 0).

$\omega_{\mathbf{q},j}$ and $\mathbf{e}_{\mathbf{q},j}$ are the frequency and polarization vector of the jth phonon branch at $\mathbf{q}$, respectively. The hyperbolic cotangent factor in Eq. (1) is related to the phonon thermal population, and it dominates the temperature dependence of the scattered intensity. The last factor in the first-order term depends on the phonon polarization. For $\mathbf{q} = (1.1, 1.1, 1.1)$ in Fig. 1, this factor is nonzero only for the longitudinal mode. Thus, the sum in Eq. (1) is reduced to a single term.

The curves in Fig. 1(a) are computed TDS intensity variations assuming a phonon frequency of 0.5, 1.5, 2.5, 3.5, and 4.5 THz, in increments of 1.0 THz. Each curve has been shifted and rescaled vertically so that the two end points match the data. Different assumed phonon frequencies lead to different shapes of the curves. The curve that best describes the data yields the phonon frequency of the mode, 2.5 THz, for the present case. An arbitrary vertical shift is implemented in this analysis because there are other contributions to the x-ray signal including Compton scattering, defect and impurity scattering, ambient scattering, etc. Inasmuch as these contributions are temperature-independent, they are effectively subtracted away. The use of an arbitrary scaling factor in the analysis sidesteps the difficulties associated with absolute intensity measurements, which can be further complicated by the presence of other contributions. Absolute intensity measurements have been implemented in previous studies [10–13], but the errors can be significant.

The shape of the data curve in Fig. 1 begins with a horizontal segment at low temperatures because the phonons are frozen out, and the TDS intensity is dominated by zero point vibrations. At higher temperatures, the intensity turns upward as the phonon population increases. The "threshold" for intensity upturning is related to the phonon frequency. This explains the differences in shapes for the different assumed phonon frequencies in Fig. 1. This dependence permits a unique determination of the phonon frequency.

For the case discussed above, a first-order analysis suffices; so do most of the other data sets to be presented below. However, high-order effects involving multiple phonon creation or annihilation can become significant for cases involving high frequency modes with correspondingly low first-order scattering intensities. The multiple phonons in a high-order process share the momentum transfer, and the mixing of $\mathbf{q}$ complicates the data analysis. For improved accuracy, we have adopted a Debye model in a calculation of the high-order contributions [6–8] using the known Debye temperature of 344 K determined from specific heat measurements [14]. The calculation is included in the data analysis as a correction term. As high-order scattering is fairly diffuse in momentum space, the Debye model is an excellent approximation, as verified by rigorous all-order calculations using the known phonon dispersion relations (such calculations are extremely time-consuming). Using the Debye model retains the

ab initio character of the method, and it is simple to implement. In our analysis, the relatively minor temperature dependence of the Debye-Waller factor is also computed within the Debye model.

Figure 1(b) shows another example of the data analysis, presented in the same manner as in Fig. 1(a). The momentum transfer is $\mathbf{q} = (2.65, 0, 0)$. Again, only the longitudinal mode contributes. This mode has a relatively high frequency, 6.4 THz, and the TDS intensity is relatively low, as evidenced by the higher relative noise level in the data compared to Fig. 1(a). Nevertheless, the frequency of the mode can be readily extracted from the data, albeit with a higher uncertainty.

Figures 2(a) and 2(b) present the same two cases again, including the data (circles) and the best fits (solid curves). The best fits, with the high-order corrections subtracted, are indicated as dashed curves and labeled as "first order only." If the first-order curve in Fig. 2(a) is appropriately shifted and rescaled in the vertical direction, it would overlap the solid curve almost exactly. As mentioned above, a first-order analysis suffices in this case. For the case in Fig. 2(b), high-order correction becomes significant, and a first-order-only analysis would give rise to an error of about 6%. In general, high-order effects can be minimized by restricting the magnitude of the momentum transfer and/or by restricting the maximum temperature of the scan.

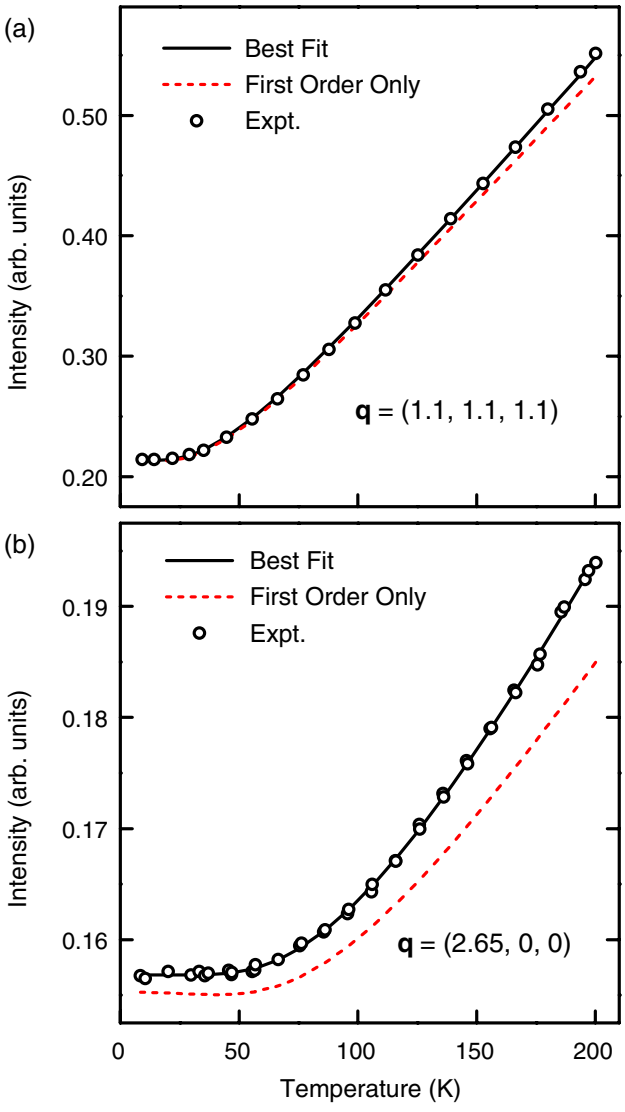

FIG. 2 (color online). Experimental and calculated TDS intensities as a function of temperature for $\mathbf{q}$ at (a) (1.1, 1.1, 1.1) and (b) (2.65, 0, 0). The intensity from first-order scattering only is also presented.

Figure 3 presents the phonon dispersion curves of Cu extracted from the experiment. The results are in excellent agreement with prior neutron measurements taken at 296 K as shown in the figure [15]. All data points include the high-order corrections, although the corrections are significant only for a few high frequency modes. It is not necessarily easy to determine *a priori* the ranges of experimental parameters that would be appropriate for a first-order-only analysis. A straightforward application of the high-order correction is perhaps the best approach, as adopted in the present study.

The two cases presented in Fig. 1 each involve just one mode because of polarization selection. To probe the corresponding transverse modes, one must select a different polarization configuration. For instance, to access the transverse mode at $\mathbf{q} = (1.1, 1.1, 1.1)$, which is equivalent to (0.1, 0.1, 0.1), the momentum transfer was chosen to be (1.9, 1.9, 0.1) in the experiment. This is again equivalent to (0.1, 0.1, 0.1), but both the longitudinal and transverse modes contribute to the TDS intensity. The analysis proceeded in the same manner, but with the longitudinal mode contribution calculated using the frequency deduced from the data at $\mathbf{q} = (1.1, 1.1, 1.1)$. For dispersion relations along the [110] direction, all three phonon branches have different dispersion relations. It is necessary to take three

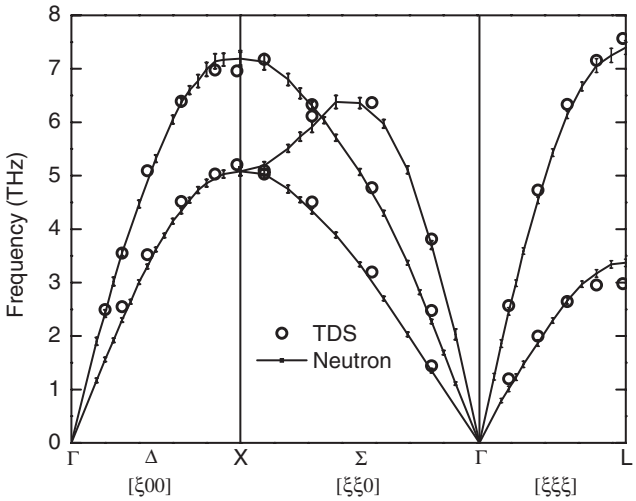

FIG. 3. Phonon dispersion relations deduced from experiment (circles). Results from prior neutron scattering measurements are shown for comparison.

data sets in order to deduce the frequencies of the three modes at each **q**.

The above results demonstrate that the method works well. Conceptually, the energy analysis in IXS is replaced by a thermal (calorimetric) analysis in the present method: the heat content in the system at each point in momentum space is characterized by the phonon populations, which are measured by x-ray TDS intensities. Since the TDS signal is derived from an energy-integrated intensity, the count rate is much higher, permitting a rapid rate of data acquisition. This method should be a useful addition to the arsenal available for studies of phonons and quantum phase transitions in solids.

This work is supported by the U.S. Department of Energy (Grant No. DE-FG02-07ER46383). We acknowledge partial support from the U.S. National Science Foundation (Grant No. DMR-05-03323) and the Petroleum Research Fund, administered by the American Chemical Society, for personnel, equipment, and beam line operations. The Advanced Photon Source, where some of the work was performed, is supported by the U.S. Department of Energy (Grant No. W-31-109-ENG-38).

*Chiang@mrl.uiuc.edu

[1] G. Dolling, *Inelastic Scattering of Neutrons in Solids and Liquids* (IAEA, Vienna, 1963).
[2] B. Dorner, E. Burkel, Th. Illini, and J. Peisl, Z. Phys. B **69**, 179 (1987).
[3] M. Schwoerer-Böhning, A. T. Macrander, and D. A. Arms, Phys. Rev. Lett. **80**, 5572 (1998).
[4] T. Ruf *et al.*, Phys. Rev. Lett. **86**, 906 (2001).
[5] M. Holt, Z. Wu, H. Hong, P. Zschack, P. Jemian, J. Tischler, H. Chen, and T.-C. Chiang, Phys. Rev. Lett. **83**, 3317 (1999); M. Y. Chou and M. Choi, *ibid.* **84**, 3733 (2000); M. Holt and T.-C. Chiang, *ibid.* **84**, 3734 (2000).
[6] R. Xu and T.-C. Chiang, Z. Kristallogr. **220**, 1009 (2005).
[7] R. Xu, H. Hong, and T.-C. Chiang, in Diffuse Scattering in the 21st Century: Emerging Insights into Materials Structure and Behavior, edited by G. Ice and R. Barabash (to be published).
[8] B. E. Warren, *X-Ray Diffraction* (Addison-Wesley, New York, 1966).
[9] J. Als-Nilesen and D. McMorrow, *Elements of Modern X-Ray Physics* (Wiley, New York, 2001).
[10] E. H. Jacobsen, Phys. Rev. **97**, 654 (1955).
[11] C. B.Walker, Phys. Rev. **103**, 547 (1956).
[12] R. Colella and B. W. Batterman, Phys. Rev. B **1**, 3913 (1970).
[13] S. S. Chang and R. Colella, Phys. Rev. B **15**, 1738 (1977).
[14] W. S. Corak, M. P. Garfunkel, C. B. Satterthwaite, and A. Wexler, Phys. Rev. **98**, 1699 (1955).
[15] E. C. Svensson, B. N. Brockhouse, and J. M. Rowe, Phys. Rev. **155**, 619 (1967).